Influence of aerodynamic characteristics of "H" beams on galloping stability.

Fernando GANDIA
Aeronautical Engineer
Universidad Politécnica de Madrid, Spain.
fernando.gandia@upm.es

Assistant Professor of Mechanics of Fluids and Aerodynamics.

Jose MESEGUER
Aeronautical Engineer
IDR/UPM. Madrid, Spain.
j.meseguer@upm.es

Professor of Aerospace Engineering

Angel SANZ
Aeronautical Engineer
IDR/UPM. Madrid, Spain.
angel.sanz.andres@upm.es

Professor of Aerospace Engineering

Summary

This paper presents the experimental study developed on a prismatic beam with "H" section, sometimes used in bridges as suspenders, vertical bars or decks.

The purpose of this study is to understand the physical behavior of the air around this type of section, in order to reduce the aerodynamic loads, the onset speed of galloping and even to avoid it. To achieve this, a study of the influence of all geometric parameters that define the section has been developed. Previously, the most interesting configurations have been selected using a smoke flow visualization technique in the wind-tunnel, then the corresponding static aerodynamic loads were measured, completed with dynamic tests and, finally, the parameters governing the phenomenon of galloping determined.

Keywords: Translational galloping instability, bluff bodies, wind tunnel, dynamic tests.

1. Introduction

It is well known that two-dimensional bluff bodies in cross-flow are subject to typical aeroelastic phenomena like vortex shedding, translational and torsional galloping, and even flutter. Galloping is a typical instability of flexible, lightly damped structures. Under certain conditions these structures may have large amplitude, normal to wind oscillations, at much lower frequencies than those of vortex shedding found in the Kármán vortex street.

Theoretical foundations of galloping are well established and can be easily understood through an extremely simple theory like the one due to Den Hartog [1], which, in a first attempt, is enough to elucidate if a given two-dimensional body can gallop or not. According to Den Hartog, galloping can be explained by taking into account that, even if the incident wind velocity U_∞ is uniform and constant, in a body reference frame the lateral oscillation of the body can cause that the total velocity experiences changes both in its magnitude and direction with time. Therefore, the body angle of attack also changes with time, hence the aerodynamic forces acting on it (figure 1).

Concerning the stability analysis, it is based on the simplest model of galloping (one degree of freedom) it is assumed that a two-dimensional body, whose mass per unit length is m, is elastically mounted on a support with a damping coefficient ζ and a stiffness $m\omega^2$ (where ω is the angular natural frequency). Within this approximation, if the aerodynamic force (proportional in this case to $\mathrm{d}z/\mathrm{d}t$) is considered as a contribution to the total damping of the system, the total damping coefficient is:

$$\zeta_T = \zeta + \frac{\rho U_\infty b}{4m\omega}\left(\frac{\mathrm{d}c_l}{\mathrm{d}\alpha} + c_d\right) \tag{1}$$

where U_∞ stands for the upstream flow velocity, and b for a transversal characteristic length of the body (figure 2).

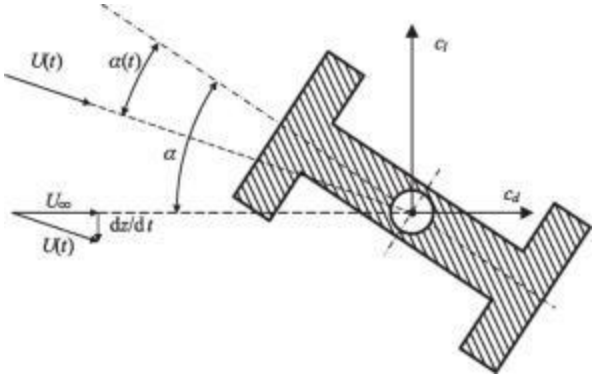

Figure 1. Sketch of a typical H beam under galloping. U_∞ is the unperturbed upstream flow velocity, dz/dt is the vertical velocity due to transversal body oscillation, α is the angle of attack of the body under static conditions, and $\alpha(t)$ the actual one. Lift and drag coefficients are c_l and c_d, respectively.

Therefore, the oscillation will be damped if $\zeta_T > 0$ and unstable if $\zeta_T < 0$. As the mechanical damping ζ is generally positive, instability will only occur if the parameter $H = dc_l/d\alpha + c_d < 0$, expression known as Den Hartog criterion, which is a necessary condition for galloping instability. The sufficient condition for galloping is $\zeta_T < 0$, or, according to equation (1) and the above definition of the parameter H, $H < -4m\zeta\omega/(\rho U_\infty b)$.

From inspection of equation (1), since the drag coefficient is positive, it is clear that the slope of the lift coefficient versus angle of attack curve must be negative, which means that the body must be stalled ($dc_l(\alpha)/d\alpha < 0$) and that the absolute value of this slope curve must be larger than the drag coefficient.

Galloping has focused the attention of many researchers during the last decades because of its impact in very common problems related to ice accretion on electric transmission lines, catenary leads, suspenders in arch bridges and other long vertical bars in truss bridges and many other two-dimensional configurations, and a fairly large number of papers dealing with the galloping properties of a wide spectrum of geometries has been published (see [2-3] for reviews on this topic). It must be pointed out that most of the effort in galloping research has been concentrated in bodies with square or rectangular cross-sections, although prismatic bodies with other cross-sectional shapes have been also considered. [4-6]

In the last years some research on galloping has been carried out at IDR/UPM, and a systematic parametric analysis of simple cross-section two-dimensional bodies has been accomplished (the geometries analysed up to now are isosceles triangular cross-sections, as well as biconvex and rhomboidal cross-sections). In this paper the transverse galloping characteristics of H shaped beams is analysed through static aerodynamic tests, measuring aerodynamic forces on the models. The aim of this study is to elucidate how the body geometry affects the galloping characteristics (figure 2), as well as the analysis of suitable geometry modifications to suppress galloping phenomena.

2. Experimental setup and procedures

2.1 Static tests

Static Tests were carried out at the Laboratorio de Aerodinámica of the E.U.I.T. Aeronáutica (Universidad Politécnica de Madrid). An open return, blown, Plint & Partners modified wind tunnel was used. It has a 8:1 contraction ratio and a rectangular test chamber of 160 mm wide, 1200 mm high and 1500 mm length. The speed in the test section can be up to 30 m/s. The turbulence intensity level is 0.7 %, and the non-uniformity of the flow less than 1 %, so that this wind tunnel becomes appropriate for low Reynolds number tests [4]

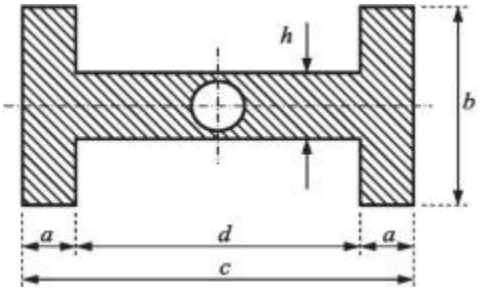

Figure 2. Parameters that define the geometry of a typical H beam.

.

For the aerodynamic forces measurement, an external, pyramidal, three components, electronic Plint Ltd. balance was used, which allow the lift and drag force to be measured, as well as the pitching moment of the body placed inside the test chamber. From Pitot tube measurement, the air flow velocity U∞ is obtained, leading to a chord based Reynolds number of 10^5,

The different models were made of Necuron® resin and machined in a Roland MDX–540 milling machine with a 0.1 mm precision. All of them are 158 mm span, thus leaving a 1 mm gap between the wind tunnel walls and the lateral surfaces of the models. It must be pointed out that this gap does not affect to the two-dimensional behaviour of the model, the reasons being that these gaps are very narrow and they are placed at the boundary layers that develop at the wind tunnel walls [5].

Furthermore, some visualization tests were performed by using a small smoke wind tunnel (the working section is 0.4 m high, 0.04 m wide and 0.6 m long), in order to get additional information on the morphology of the flow past the models.

In experiments the lift, $l(\alpha)$, drag, $d(\alpha)$, and pitching moment, $m(\alpha)$, were measured at angles of attack varying form $\alpha = 0º$ to $\alpha = 90º$ at variable $\Delta\alpha$ step (this step is smaller, $\Delta\alpha = 1º$, where the lift slope curve is negative, and galloping can occur, and larger, $\Delta\alpha = 5º$, where the lift slope is positive). From measured results the aerodynamic coefficients are determined, $c_l(\alpha) = l(\alpha)/(q_\infty c)$, $c_d(\alpha) = d(\alpha)/(q_\infty c)$, $c_m(\alpha) = m(\alpha)/(q_\infty c^2)$, and then the Den Hartog parameter $H = \mathrm{d}c_l/\mathrm{d}\alpha + c_d$ is calculated.

2.2 Dynamic tests

The dynamic tests were carried out at IDR/UPM. An open return wind tunnel, A4C, has been used. A4C wind tunnel has a rectangular test section 0.2 m wide, 1.8 m high and 2 m length. The turbulence intensity at the tests section is under 3%, and the non-uniformity of the flow is less than 2 %. The models chord is c = 0.2 m and the height b = 0.1 m. Models span is 0.196 m.

As sketched in figure 3, the model M, located inside the wind tunnel test chamber, between the wind tunnel walls W, is anchored to the sliding support S through the rod R. The support S can move vertically along the two steel columns C, so that to allow the vertical displacement of the rod there is a vertical slot in the corresponding test chamber wall. The support device is equipped with air lubricated bushings in order to reduce mechanical friction as much as possible. Two springs limit the vertical amplitude of the oscillation movement of the model. These springs are interchangeable to adjust the stiffness of the system, thus allowing to fix the onset velocity of galloping within the wind tunnel velocities range.

The rod R is attached in such a way that the angle of attack of the model can be set from 0º to 90º with ±0,5º accuracy. The vertical displacement is measured with a laser sensor L (MEL model M7L100) with 100 mm measuring range and 64 μm resolution. As already said, the model, as well as part of the rod, is located inside the wind tunnel test chamber, whereas the oscillation mechanism and instrumentation are outside the test chamber, all this external equipment being enclosed a tight box which is kept at the test chamber pressure because of the vertical slot.

Once the stiffness of the system is experimentally measured, the angular natural frequency ω and the structural damping ζ are determined letting the model vibrate freely at cero wind speed. By comparing the residence time of a fluid particle, $t_r \sim c/U_\infty$, with the characteristic time $t_o \sim 1/\omega$, the condition for almost static criterion is obtained. that is $t_r << t_o$, or $U_\infty >> c\omega$

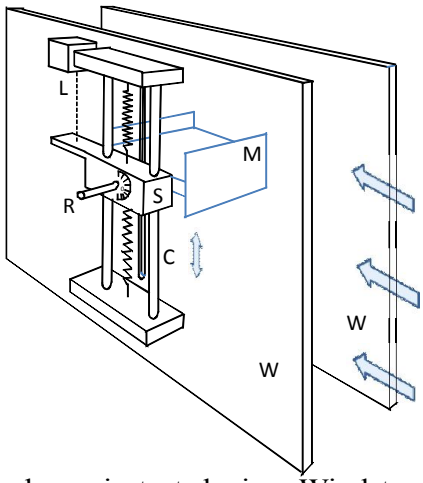

Figure 3. General view of the dynamic test device. Wind tunnel walls (W), model (M), rod (R), sliding support (S), columns (C), laser displacement sensor (L).

3. Experimental results

3.1 Static tests.

In the case of static tests, two types of H-section beam configurations were considered. In all cases the lengths c and b were kept constant. In the first type, type I, the length a was varied from $a/c = 0.015$ to $a/c = 0.50$ (this last configuration corresponds to a rectangular beam), the aim of these tests being to study the influence of thickness of the extreme vertical plates on the galloping behaviour.

In the second set of H beam configurations, type II, the thickness a was kept constant ($a/c = 0.015$), but holes of different diameters were drilled on the vertical plates to modify its porosity. The porosity is defined as the ratio to the frontal surface of the drilled portion of the vertical plates, that is $(b - h)s$, were s stands for the model span, of the surface of the holes made in such a surface, $\phi = \pi nr2/[(b - h)s]$, n being the number of holes made in the span s and r the hole radius.

The results obtained with the type I beams are depicted in the left column of figure 4, whereas results corresponding to porous H beams (type II) are shown in the right column of the same figure 3.

Concerning type I beams, the results show that the lift slope becomes negative close to $\alpha = 0º$ until it reaches a minimum at $\alpha \cong 6º$ (the beam is stalled), this behavior being the same independently of the value of the parameter $2a/c$, beyond this minimum the lift coefficient start to grow as the angle of attack grows, so that the lift coefficient slope curve becomes positive. Form the point of view of galloping there is another region, close to $\alpha = 90º$, where the lift slope becomes again largely negative.

The drag coefficient increases as the angle of attack grows in almost all the whole range ($0º \leq \alpha \leq 90º$) except close to $\alpha \cong 65º$ where relative minima appear no matter the value of the parameter $2a/c$ is. These local minima coincide with the angles of attack where the lift slopes start to be almost constant and largely negative (figure 4).

To get some additional insight on this behavior some visualization in a small smoke wind tunnel were performed, and some of the pictures obtained are shown in figure 5. Note that for $\alpha < 55º$ the upper boundary layer separates at the upper leeward corner of the H beam, whereas for $\alpha > 75º$ the separation takes place at the upper windward corner. For $\alpha \cong 65º$ smoke streamlines are parallel to the H beam upper surface, which probably implies a narrow wake behind the body at these values of the angle of attack.

With the experimental results related to c_l and c_d, the Den Hartog function $H = dc_l/d\alpha + c_d$ has been determined, and represented in figure 4. As it can be observed, there is a region close to $\alpha = 0º$ where H beam configurations are unstable (see also figure 6), and there is another region close to $\alpha = 90º$ where these bodies are weakly unstable. Between these two regions H beams are not prone to transversal galloping oscillations. It must be remarked that for large values of the angle of attack,

although according to Den Hartog criterion the H function is negative, the absolute values of this parameter are so small that the resulting motions are only marginally unstable.

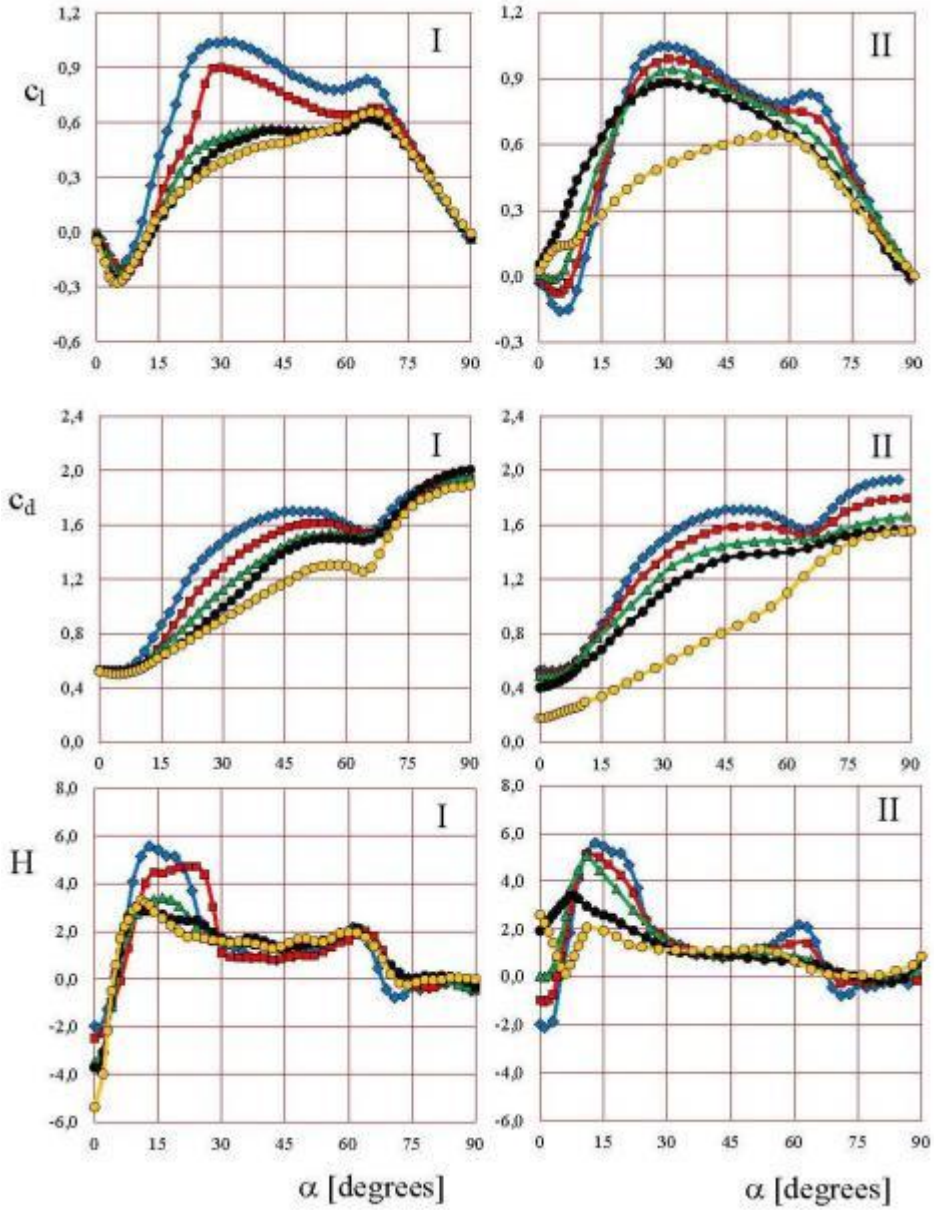

Figure 4. Variation with the angle of attack, α, of the lift coefficient, c_l, the drag coefficient, c_d, and the Den Hartog parameter $H = dc_l/d\alpha + c_d$. Left column, type I H beams (solid vertical plates) with different $2a/c$ ratio (the symbols identify the values of the parameter $2a/c$ according to the key: $2a/c = 1$, yellow circles; $2a/c = 0.8$, black circles; $2a/c = 0.6$, green triangles; $2a/c = 0.2$, red squares; $2a/c = 0.03$, blue rhombi). Right column, type II H beams, with fixed $2a/c = 0.06$ and $b/c = 0.5$ values, but with vertical plates with different porosities (the symbols identify the values of the parameter ϕ according to the following key: $\phi = 1$, yellow circles; $\phi = 0.6$, black circles; $\phi = 0.4$, green triangles; $\phi = 0.2$, red squares; $\phi = 0$, blue rhombi).

Note that the unstable region must be almost the same for $2a/c = 0$ and $2a/c = 1$, provided the chord c is large enough (in both cases the H beam behaves as a rectangular cross section body).

The differences between the tested type II H beams are in the porosity ϕ of the vertical plates (when $\phi = 0°$), which was changed from $\phi = 0$ (solid vertical plates, yellow circles in the right column of figure 3) to $\phi = 1$ (no vertical plates, blue rhombi). The measured results, c_l, c_d and H versus ϕ are shown in figure 4. According to these plots, it seems that H beams are stable for large enough

values of the porosity, both for small and large values of the angle of attack (figure 6).

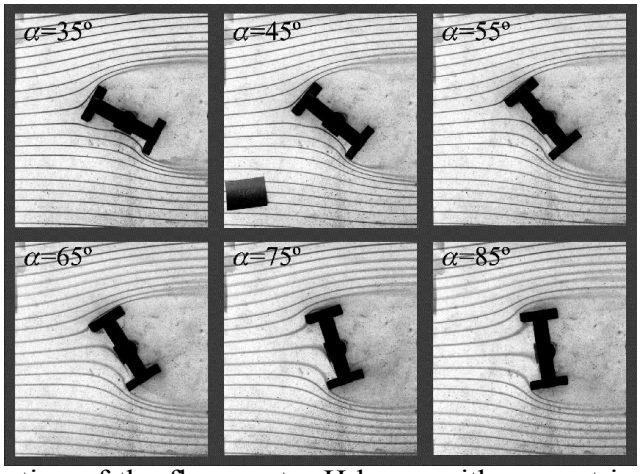

Figure 5. Smoke visualization of the flow past a H beam with geometrical parameters $2a/c = 0.25$ and $b/c = 0.45$. From Gandía et al. [6]

Gallop absence for large porosities, say greater than $\phi = 0.4$, can be explained by the fact that the central core of the H section, without the vertical plates, is a rectangular section with $h/d = 0.25$ (see figure 2) which is no prone to gallop [7].

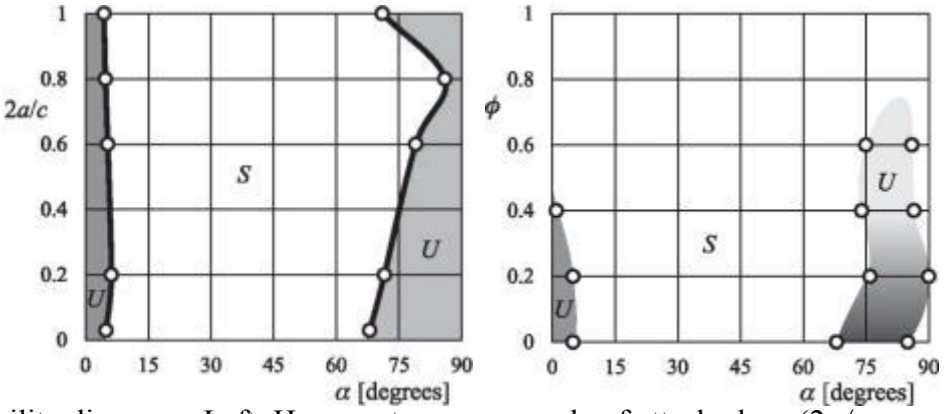

Figure 6. Stability diagrams. Left: H geometry versus angle of attack plane ($2a/c$ vs. α plane). Right: Stability diagram of H beams in the porosity versus angle of attack plane (ϕ vs. α plane), corresponding to H beams with $2a/c = 0.06$ and $b/c = 0.45$, where the lengths a, b and c are defined in figure 2. Shadowed areas indicate unstable regions.

3.2 Dynamic tests

The second set of H beam configurations, type II, with $c/b = 2$, was selected (now $a/c = 0.025$), with the objective of verify the Den Hartog criterion for values of porosity 0, 0.2 and 0.4. Figure 7 shows the root mean square (rms) of the maxima of the dimensionless vertical amplitude, z/b, as a function of the reduced velocity, $U_{red} = U_\infty/(\omega b)$, for zero angle of attack.

Here z stands for the vertical amplitude and b for the frontal height b of the H section beam

Note that at this angle of attack, gallop appears only when $\phi = 0$. For higher porosities the prism has only a small amplitude oscillation. Note also the hysteresis region that appears in $\phi = 0$ configurations (additional details on the hysteresis of the response of galloping bodies can be found in [7-9].

The results obtained for the three porosities, varying the angles of incidence from 0º to 90º, are also depicted in figure 7. It can be seen that for angles of attack close to zero degrees, the instability region is substantially reduced, and the galloping phenomenon disappears provided the porosity

becomes larger than 0.1. Close to 90º, galloping instability completely disappears when dynamic test are considered, at least in the range of wind speeds of experiments.

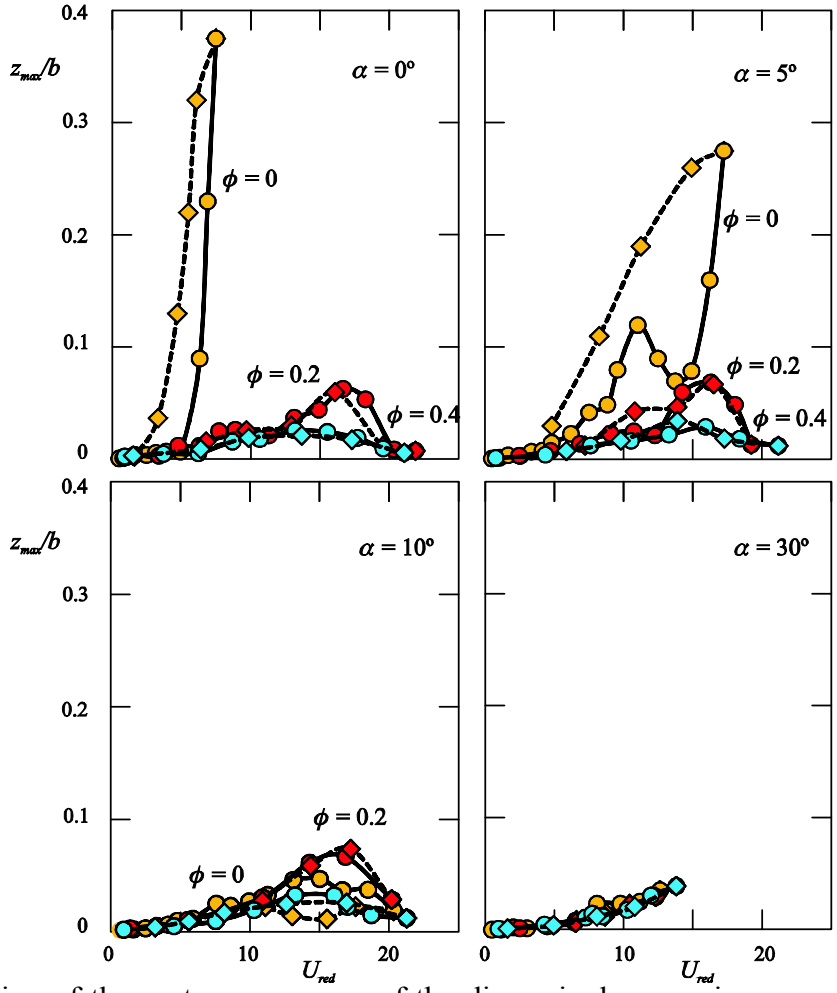

Figure 7. Variation of the root mean square of the dimensionless maximum oscillation amplitude, z/b, with the reduced speed, $U_{red} = U_\infty/(\omega b)$, at zero angle of attack, for three values of the porosity ϕ. Circles correspond to test series where the reduced velocity increases, whereas rhombi indicate decreasing reduced velocity.

The reduction in the size of the instability region shown in figure 7 can be explained because of the mechanical dissipation involved in an oscillation mechanism (even if air bushing are used), as well as of the higher turbulence existing in the flow of the wind tunnel used in the dynamic tests when compared with one existing in the wind tunnel used in the static tests. It is well known, that for rectangular sections the turbulence increases the mixing in the shear layer of the separated region, reducing the suction peak in the lower surface at low angle of attack [2, 10, 11]. This cause a reduction in the galloping effects and for higher values of turbulence the galloping is eliminated.

4. Conclusions

This paper describes an experimental procedure to analyse the influence of several geometric parameters on the galloping behaviour H cross-section beams. Although the analysis has been constrained to a few geometrical configurations, experimental results show that, for the configuration under study, the influence of the parameter $2a/c$ do not substantially affects the phenomenon of galloping. On the other hand, porosity, ϕ, seems to be an important parameter to effectively control the galloping behavior.

The results of the dynamic tests show that the region of unstable configurations in the ϕ versus α plane is smaller than the one obtained when the static Den Hartog criterion is applied, as one could

expect taking into account previous results concerning the galloping behaviour of triangular cross-section bodies published elsewhere [12]

For this type of H sections, a noticeable effect of the stream turbulence has been found. In this sense, the turbulence effect on the analysed H section bodies seems to behave in a similar way as in rectangular section bodies.

5. References

[1] J. P. Den HARTOG, *Mechanical Vibrations*, 4th ed. New York: Mc Graw Hill, 1956.

[2] R. D. BLEVINS, *Vibration of Structures Induced by Fluid Flow*, 2nd ed. New York: Van Nostrand Reinhold, 1990.

[3] E. NAUDASCHER and D. ROCKWELL, *Flow-Induced Vibrations: An Engineering Guide*. Rotterdam: A.A. Balkema, 1994.

[4] J. B. BARLOW, W. H. RAE, and A. POPE, *Low-Speed Wind Tunnel Testing*, 3rd ed. New York: John Wiley & Sons Inc., 1999.

[5] L. AYUSO, R. SANT, and J. MESEGUER, "Influence of Leading Edge Imperfections on the Aerodynamic Characteristics of NACA 63(2)215 Laminar Aerofoils at Low Reynolds Number," *Proc. IMechE, Part G J. Aerosp. Eng.*, 2013.

[6] F. GANDIA-AGUERA, J. MESEGUER, and A. SANZ-LOBERA, "Experimental Study of the galloping stability of H-sections beams," in *5th European Conference for Aeronautics and Space Sciences (EUCASS). July 1-5*, 2013.

[7] M. P. PAÏDOUSSIS, S. PRICE, and E. LANGRE, *Fluid–Structure Interactions: Cross-Flow-Induced Instabilities*. Cambridge University Press, 2011.

[8] G. ALONSO, A. SANZ-LOBERA, and J. MESEGUER, "Hysteresis phenomena in transverse galloping of triangular cross-section bodies," *J. Fluids Struct.*, vol. 33, pp. 243–251, Aug. 2012.

[9] G. ALONSO, E. VALERO, and J. MESEGUER, "An analysis on the dependence on cross section geometry of galloping stability of two-dimensional bodies having either biconvex or rhomboidal cross sections," *Eur. J. Mech. - B/Fluids*, vol. 28, no. 2, pp. 328–334, Mar. 2008.

[10] P. HÉMON, F. SANTI, B. SCHNOERRINGER, and J. WOJCIECHOWSKI, "Influence of free-stream turbulence on the movement-induced vibrations of an elongated rectangular cylinder in cross-flow," *J. Wind Eng. Ind. Aerodyn.*, vol. 89, no. 14–15, pp. 1383–1395, Dec. 2001.

[11] Z. Q. CHEN, G. D. LIU, and M. G. LIU, "Wind-Resistant Characteristics of H-Shape Slender Hangers," in *7th Asia-Pacific Conference on Wind Engineering*, 2009.

[12] G. ALONSO, J. MESEGUER, and I. PÉREZ-GRANDE, "Galloping instabilities of two-dimensional triangular cross-section bodies," *Exp. Fluids*, vol. 38, no. 6, pp. 789–795, Apr. 2005.